Clays and Clay Minerals, Vol. 57, No. 1, 25–34, 2009.

X-RAY DIFFRACTION LINE-BROADENING STUDY ON TWO VIBRATING, DRY-MILLING PROCEDURES IN KAOLINITES

PABLO PARDO[1,2,*], JOAQUÍN BASTIDA[1], FRANCISCO J. SERRANO[1], RAFAEL IBÁÑEZ[2], AND MAREK A. KOJDECKI[3]

[1] Departamento de Geología, Universidad de Valencia, 46100 Burjasot, Valencia, Spain
[2] Instituto de Ciencia de Materiales, Universidad de Valencia, P.O. 22085 46071 Valencia, Spain
[3] Instytut Matematyki i Kryptologii, Wojskowa Akademia Techniczna, 00-908 Warszawa, Poland

Abstract—Due to the great technological importance of the microstructure of kaolinite, characterizing its evolution during dry milling of kaolin and analyzing the microstructural information obtained from different methods were the main aims of this work. The microstructural alteration of kaolinite is evaluated by X-ray diffraction and electron microscopy methods, comparing the results obtained and analyzing the correlations between them. The Warren-Averbach and Voigt-function methods of X-ray diffraction microstructural analysis have been applied successfully to the study of the effects of two different, vibrating-cup dry-milling configurations in the microstructure of kaolinite from the reflections corresponding to (00l) diffracting planes. The crystallite-size estimates obtained from the two methods correlate well. Field emission scanning electron microscopy measurements of kaolinite particle thickness are in good agreement with the crystallite size estimated by the two methods. The Warren-Averbach method also provided estimates of the contribution to line broadening. Vibrating-cup milling has been proved to be a more efficient method of strain comminution of kaolinites than other milling techniques, reaching extensive microstructural degradation within seconds.

Key Words—Crystallite Size, Electron Microscopy, Kaolinite, Line Broadening, Mechanical Treatment, Strain, X-ray Diffraction.

INTRODUCTION

Mechanical treatment is one of the processes applied to many industrial minerals in order to achieve the most suitable properties for their final use. Kaolin shows a wide range of applications (Konta, 1995); it is used as a filler in paper, paints, rubber, plastics, adhesives, but it is also a raw material in traditional and technical ceramic (Marchese *et al*. 2000). Kaolin consists of aggregates of randomly oriented stacks of kaolinite flakes, known as 'books,' 'accordions,' or 'worms' (Harben and Bates, 1990). Most kaolin applications rely on the size and shape of the individual flakes. Different mechanical treatments are used to break the aggregates in order to increase the number of individual flakes, thereby modifying the physicochemical behavior of kaolinite.

The structure of kaolinite ($Al_2Si_2O_5(OH)_4$) has been studied by many authors (Murray *et al*. 1993); Bish (1993) applied Rietveld refinement to data from 1.5 K neutron diffraction experiments, concluding that it belongs to the *C*1 space group if some random positional disorder of the H atoms is assumed. Kaolinite is a (1:1) dioctahedral layer silicate. Its structure consists of layers, each one comprising one tetrahedral siloxane sheet and one octahedral gibbsite-type sheet. The layers are bonded together in the '*c*' direction by hydrogen bonds between the hydroxyl groups in the gibbsite basal plane of one layer and the oxygen of the siloxane sheet of the next layer.

Dry-grinding leads to the delamination of kaolinite (Sánchez-Soto *et al*., 2000), due to the breakage of the weak hydrogen bonds between the layers. This effect can be observed with X-ray diffraction (XRD) measurements, where the intensity of 00l reflections decreases with grinding time (Kristóf *et al*., 1993; Makó *et al*., 2001; Frost *et al*., 2001). Qualitative and quantitative observations by field emission scanning electron microscopy (FESEM) and atomic force microscopy (AFM) are also possible, as performed by Zbik and Smart (1998). Infrared (IR) spectroscopy (Frost *et al*., 2002) and specific surface area measurements with nitrogen adsorption are also common methods in the study of the effects of mechanical treatment of kaolinite (González-García *et al*., 1991).

Transverse breakage of particles through fractures parallel to the *c* axis was also observed in mechanical treatment of kaolinite (Baudet *et al*., 1999); grinding equipment and operating parameters were found to affect the predominance of delamination over transverse breakage.

Clausell *et al*. (2007) applied a method allowing easy measurement of the thickness of kaolinite particles (flakes), reported as crystallites, from FESEM images, finding good correlation between these values and those of XRD average apparent crystallite sizes from 001 reflections estimated by the Voigt function method. Those authors worked with a set of samples selected from a wide survey (Clausell, 2001) of XRD micro-

* E-mail address of corresponding author:
pablo.pardo@uv.es
DOI: 10.1346/CCMN.2009.0570102

structural characteristics of kaolinites in the Iberian Massif (Spain).

A study of the influence of the microstructure of kaolinite on the efficiency of milling processes (Pardo *et al*., 2007) confirmed that poorly crystallized materials (from Queensland), with small average apparent crystallite sizes, yielded poorer efficiencies (considered as the slope of linearized crystallite size *vs*. milling time) than well crystallized ones. High-energy, vibrating-cup milling was also established to be a more efficient comminution method than attrition or planetary-ball milling techniques applied to the same reference kaolin KGa-1 (Sánchez-Soto *et al*. 2000) or to a Slovakian kaolin (Frost *et al*., 2001) that needed longer times to achieve significant microstructural changes.

The aim of this study was to improve the evaluation of microstructural changes in dry grinding of kaolinite. Two different methods of XRD line-broadening analysis were applied to KGa-1 reference kaolinite milled with two sets of a high-energy, dry-grinding, vibrating-cup mill.

MATERIALS

The material studied was the reference kaolin KGa-1, obtained from the Source Clays Repository of The Clay Minerals Society (hosted by Purdue University, West Lafayette, Indiana). This material has been studied widely; information about the origin, physical and chemical characteristics, electron microscopy (SEM, TEM, AFM) images, IR spectrum, powder XRD data, and thermal analysis can be found in papers by Pruett and Webb (1993), Sánchez-Soto *et al*. (2000), Vogt *et al*. (2002), Zbik and Smart (1998), and Serrano *et al*. (1996). Its mineralogical characterization (Chipera and Bish, 2001) revealed the presence of 3 wt.% anatase.

METHODS

Experimental procedure

A Fritsch Pulverisette 9 vibrating-cup mill was used for dry grinding 10 g samples of the reference material which had been passed through a 230 μm mesh sieve. Two sets of samples were prepared; the first one using a 50 mL agate grinding set (cup and cylinder) and the second one using a 100 mL tungsten carbide coated stainless steel set of cup, ring, and cylinder. Due to the different efficiency of both configurations, milling times were slightly different in the two sets; samples were labeled with the symbol of the grinding set used and the milling time in seconds: agate set: A6, A12, A24, A36, A60; tungsten carbide-coated stainless steel set: S3, S6, S12, S24, S36. K0 refers to an untreated sample.

X-ray diffraction

The equipment used for XRD characterization was a Bruker D5000 diffractometer with CuKα radiation at 40 kV and 30 mA, Ni filter, 1º divergence slit, 1º antiscatter slit, graphite diffracted-beam monochromator, and scintillation detector. General identification was performed with a step scan ranging from 5º to 65º2θ, with 0.04º2θ step size and 8 s counting time for each sample. Microstructural analysis of 00l profiles required scans from 11 to 13.5º2θ (for 001 reflection) and from 24 to 26º2θ (for 002 reflection) with a step size of 0.01º2θ and longer counting times (12 and 18 s, respectively, for the 001 and 002 profiles).

Diffraction data were analyzed with the *Diffrac-Plus* software suite of Bruker AX Systems.

X-ray diffraction microstructural analysis

The XRD profiles of 00l basal-plane reflections were selected for microstructural analysis due to the morphological importance of these planes in terms of the shape (Olivier and Sennett, 1973) and due to their relatively high intensity and the lack of overlapped neighboring peaks.

The *Profile* software (Socabim, Bruker AXS) was used to fit experimental profiles of 001 and 002 kaolinite reflections to split Voigt functions, so that the characteristics of $K\alpha_1$ profiles were obtained. In the case of the 002 reflection, the kaolinite peak was separated from a neighboring peak of anatase at ~25.25ºθ ($CuK\alpha_1$). Instrumental profiles were simulated from the experimental scans of LaB_6 powder (NIST SRM660a) and used to obtain pure-line profiles by deconvolution. Values of reliability for profile fitting (R_{wp}) were always <3%.

The Warren-Averbach method (Bertaut, 1950; Warren and Averbach, 1950; Warren, 1955) was used in conjunction with the *Wincrysize* software (Bruker AXS) to obtain area-weighted apparent crystallite-size values (measured as unit-cell column lengths (L) in the direction perpendicular to diffraction planes considered to be (001)) by double-line analysis of 001 and 002 reflections. Based on the expression of pure (i.e. physically broadened) profiles as Fourier series, this method needs two orders of the same reflection, does not assume a specific shape for diffraction profiles, separates stress and size contributions to the XRD peak broadening, and allows the user to obtain crystallite-size distributions.

For the Voigt function method (Langford, 1978, 1992) only one line is needed and it was applied to 00l reflections, using the procedure shown by De Keijser *et al*. (1983). This method was applied successfully to another reference clay mineral (Source Clays Repository, Sep-Nev1 sepiolite) by Bastida *et al*. (2006). This simplified microstructural-analysis method provides a value of an average volume-weighted apparent crystallite size and separately an average apparent strain value.

Field emission scanning electron microscopy

FESEM images were obtained using an Hitachi 4100 field emission scanning electron microscope, working with an accelerating voltage of 30 kV. Samples were

https://doi.org/10.1346/CCMN.2009.0570102 Published online by Cambridge University Press

prepared either as a powder or an oriented aggregate (Clausell *et al*., 2007) which was placed on the FESEM holder then coated with Au-Pd using a Struers Epovac device. Digital images were then collected with the aid of the *EMIP* program (supplied by Hitachi). Particle thickness of kaolinite flakes (platelet-like particles) was measured directly from the digitized images using the *ImageJ* program, following the method of Clausell *et al*. (2007). Measurements were performed for extreme and intermediate values for both sets of samples.

RESULTS AND DISCUSSION

The 001 and 002 diffraction profiles for both sets of samples (Figure 1, Table 1) revealed that the changes in shape and intensity of the diffraction peaks with grinding time reflect the microstructural evolution of the material. Little asymmetry of experimental line profiles was observed in samples with a lower degree of crystallinity caused by the degradation of the microstructure during the milling process. This does not influence the results of microstructural analysis due to the split Voigt fitting function used, which considers the left and the right sides of the peak separately from its maximum.

According to Frost *et al*. (2001) and Makó *et al*. (2001), dry grinding breaks the hydrogen bond between adjacent kaolinite layers, leading to the delamination of the material. Another effect of dry grinding in kaolinite is the dehydroxylation of basal surfaces by the coalescence of two hydroxyl groups to form H_2O, leaving a chemically bonded oxygen as an oxide anion in the lattice (Frost *et al*., 2004). These processes contribute to the loss of the long-range order clearly observed in the 00l profiles of sample S36, which contains only a broad band centered at 12.3 and another at 24.8º2θ The proportion of amorphous material increases with grinding time, as can be concluded from the general loss of intensity and from broadening of the profiles. The degree of broadening increases with grinding and is clearly greater for samples ground with the stainless steel set, which is more effective in terms of energy due to the larger mass of the steel elements and the volume of the cup. For samples treated with the agate set, finding significant differences in the integral breadth (β_{int}) of the profiles requires longer milling times. As expected, pure 002 profiles are wider than 001 profiles due to a greater influence of strain on the second-order reflection.

Microstructural analysis (Table 2) using the Warren-Averbach method yielded values for the average column length ($<L>$), full width at half maximum of L distribution (FWHM(L)), and strain at average column length (SACL). The Voigt function method produced the values of $<D_v>$ and e, which correspond to the volume-

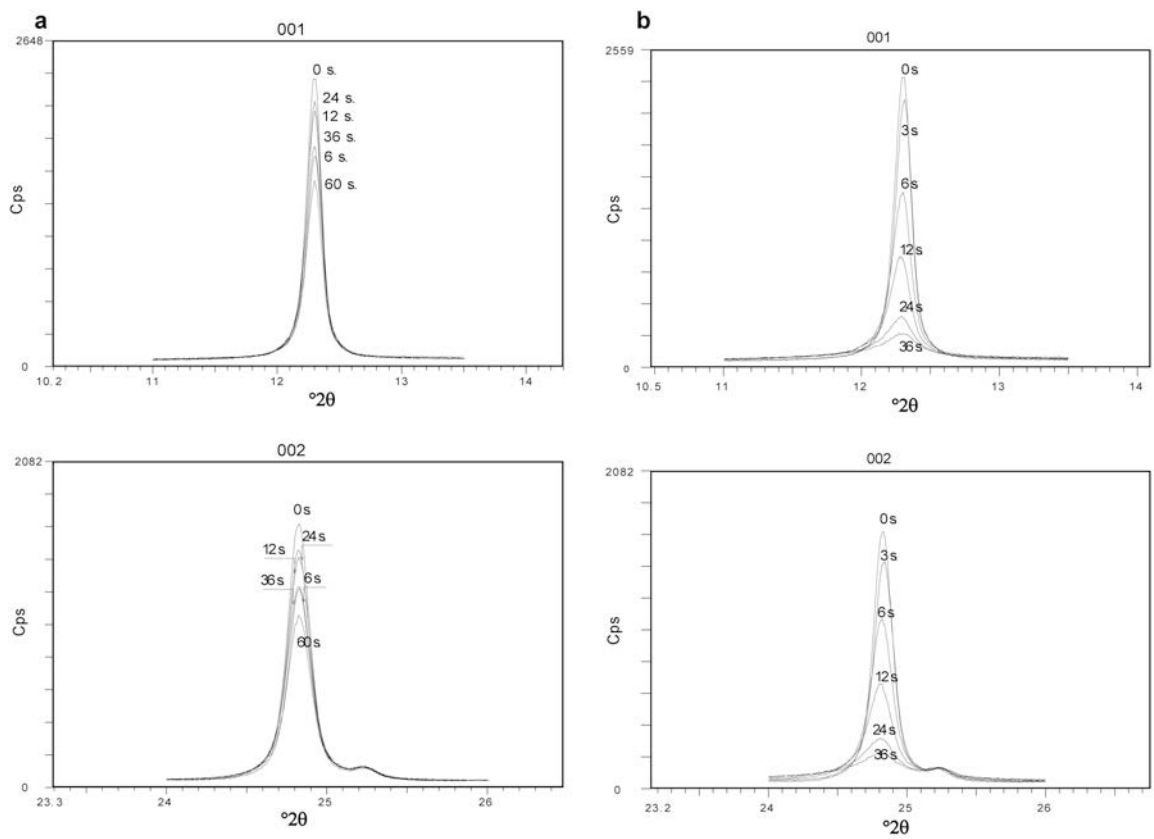

Figure 1. (a) 001 and 002 diffraction profiles for samples A; and (b) 001 and 002 diffraction proiles for samples S.

https://doi.org/10.1346/CCMN.2009.0570102 Published online by Cambridge University Press

Table 1. Data obtained from XRD profile fitting.

hkl	Sample	Position of the maximum (º2θ)	Normalized area under the curve (cps º2θ)	Intensity of the peak maximum (cps)	FWHM (º2θ)	β_{int}, Integral breadth (º2θ)	ϕ, peak shape factor (FWHM/β_{int})
001							
	STD*	12.364	2636	40030	0.055	0.066	0.835
	K0	12.294	294	1598	0.133	0.184	0.723
	A6	12.298	221	1136	0.139	0.195	0.714
	A12	12.303	263	1390	0.136	0.189	0.718
	A24	12.293	274	1451	0.134	0.189	0.709
	A36	12.281	241	1193	0.144	0.202	0.711
	A60	12.286	206	994	0.143	0.207	0.690
	S3	12.302	279	1460	0.136	0.191	0.712
	S6	12.286	215	925	0.154	0.233	0.661
	S12	12.267	139	549	0.170	0.253	0.671
	S24	12.262	88	209	0.269	0.422	0.637
	S36	12.259	66	129	0.323	0.508	0.636
002							
	STD	24.866	3364	47796	0.059	0.064	0.920
	K0	24.811	236	1248	0.137	0.189	0.726
	A6	24.817	182	928	0.141	0.196	0.719
	A12	24.820	202	1060	0.141	0.191	0.739
	A24	24.811	214	1107	0.139	0.193	0.720
	A36	24.797	185	910	0.146	0.203	0.719
	A60	24.795	174	792	0.145	0.220	0.659
	S3	24.818	205	1062	0.143	0.193	0.741
	S6	24.795	188	783	0.158	0.241	0.656
	S12	24.292	136	430	0.201	0.316	0.636
	S24	24.781	71	164	0.277	0.435	0.636
	S36	24.777	62	109	0.362	0.569	0.637

*STD – values of the instrumental profile obtained using the LaB_6 powder (NIST SRM660a) standard.

weighted average apparent crystallite size and apparent strain parameters, respectively. The error estimation was performed by applying the error propagation law to the Voigt function method considering the standard deviation of intensity values of the diffraction profiles calculated as per Klug and Alexander (1974).

For samples milled using the agate set, for up to 12 s, no clear trends in either $<L>$ or $<D_v>$ were found, as the differences between samples ground with subsequent milling times were too short. Significant differences can only be established between the first and the last two samples. A slight increase in SACL with milling time was observed, which was related to the increase in dislocations in kaolinite caused by dry grinding. This effect was not observed in the values of *e* (strain parameter) from the Voigt function method. As described by Langford (1978, 1992), this method assumes that the strain contribution to profile broadening is Gaussian. The poor Gaussian contribution to the pure $K\alpha_1$ profiles of the samples in this study was also confirmed by shape-factor values, which were closer to a pure Lorentzian ($\phi = 2/\pi = 0.6366$) than to a Gaussian function ($\phi = 2(\ln 2/\pi)^{1/2} = 0.9394$). As a consequence, the Voigt function method failed to model properly the system studied here.

The stainless-steel milling set exhibited greater efficiency, with a significant decrease in $<L>$ and $<D_v>$. The distribution of *L* became narrower, as indicated by the evolution of FWHM(*L*) (Table 2). Strain increased by an order of magnitude, again considering SACL as a more reliable strain parameter.

Evolution of *L* with grinding time (Figure 2) revealed a slight linear decrease in $<L>$ for the agate set whereas the stainless steel set produced greater efficiency, with an approximately exponential plot that reached smaller values of $<L>$ in shorter milling times.

Kaolinite comminution by the equipment used was more efficient than that achieved by either attrition or planetary-ball milling techniques, as used by Sánchez-Soto *et al*. (2000) and Frost *et al*. (2001).

The evolution of distributions of relative frequency curves of crystallite size obtained with the Warren-Averbach method for the two sets of samples (Figure 3) showed a logarithmic-normal size distribution which is

https://doi.org/10.1346/CCMN.2009.0570102 Published online by Cambridge University Press

Table 2. Results from XRD microstructural analysis (Warren-Averbach method).

Sample	<L> Average column length (Å)	FWHM (L) Full width at half maximum of L distribution (Å)	SACL Strain at average L value (Voigt function method) (10^{-3})	<D_V> (Å)	E (Estimate of error) (%)	e Strain in 001 direction (10^{-3})
K0	399	654	0.26	793	0.73	2.65
A6	357	548	–	706	1.10	2.62
A12	379	596	0.33	747	0.84	2.63
A24	366	544	0.35	715	0.74	2.35
A36	347	553	0.38	668	0.95	2.71
A60	317	428	0.54	591	1.08	2.00
S3	370	569	0.60	718	0.72	2.49
S6	269	318	0.58	465	0.90	0.77
S12	207	221	1.23	438	1.37	1.94
S24	120	140	1.60	225	4.96	–
S36	85	100	3.95	184	7.16	–

typical of small particles (particularly crystallites) of polycrystalline materials formed under specific thermodynamic and chemical conditions (Eberl *et al*., 1998). This is an approximate characteristic because in some samples the size distributions appear to be bimodal logarithmic-normal, originating from two different processes of kaolin formation. Further probing of this phenomenon was considered to be outside the scope of the present study.

For the agate set (Figure 3a), a slight evolution was observed from the K0 sample to the A60 sample in which a decrease in intensity of the secondary maximum (corresponding to larger values of L) in favor of the main maximum (centered at 160 Å) was observed. In the stainless steel set of samples, however, a much clearer trend was observed. The distribution narrowed, the secondary maximum disappeared after 12 s of milling, and the main maximum shifted to smaller L values with a progressive increase in frequency with increasing milling time. In terms of crystallite size, in the first stages of dry milling, larger crystallites were broken,

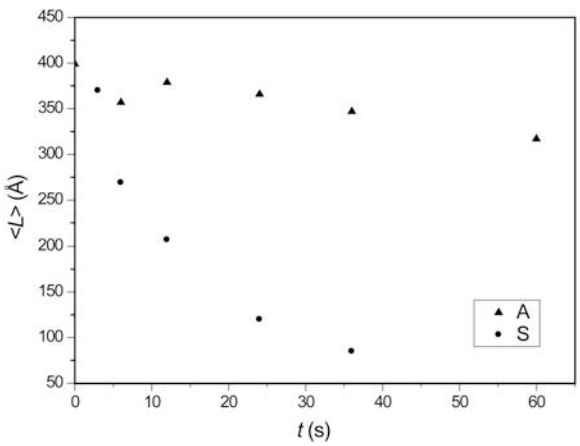

Figure 2. Evolution of <L> with grinding time for both series.

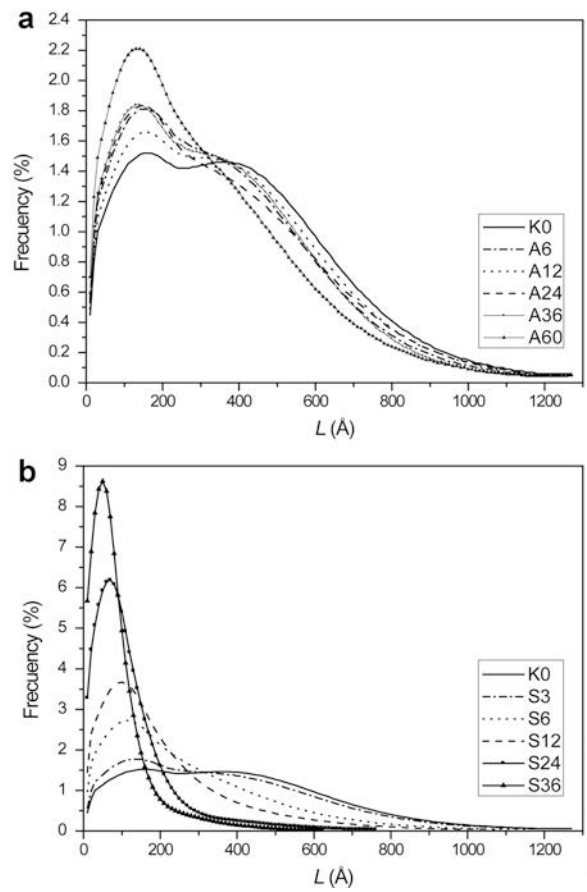

Figure 3. (a) L distribution expressed in relative frequency for samples milled with the agate set (A); (b) L distribution expressed in relative frequency for samples milled with the stainless steel set (S).

https://doi.org/10.1346/CCMN.2009.0570102 Published online by Cambridge University Press

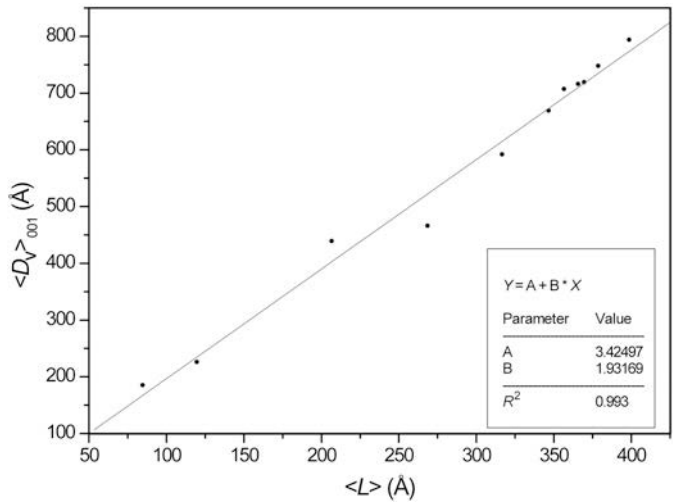

Figure 4. Correlation plot between $<D_v>$ and $<L>$.

adding the fragments to the intermediate and smaller fractions. Then, as milling time increased, these smaller crystallites were also affected, leading to a monomodal distribution that shifted its maximum to smaller L values.

From the correlation plot of $<D_v>$ *vs.* $<L>$ (Figure 4), the $<L>$ values obtained using the Warren-Averbach method were found to be smaller than $<D_v>$ values provided by the Voigt function method. This was also reported by Langford (1992). A good correlation (R^2 = 0.993 for $<D_v> \approx 1.9 <L>$) between the two microstructural parameters was observed (Figure 4), as expected based on previous studies dealing with mullites and kaolinites (Serrano *et al.*, 1996; Clausell, 2001; Clausell *et al.*, 2007). The ratio of volume-weighted $<D_v>$ to surface-weighted $<L>$ coherent domain sizes is in the range of that proposed (1.3−2.0) by Balzar and Ledbetter (1993).

In kaolin, due to its tendency to delaminate parallel to (001) crystalline planes, the crystallites are probably either small plates or tightly connected prisms that are aggregated as mosaic blocks into plate-like crystalline grains of the same thickness in a direction perpendicular to the (001) planes. Under such an assumption, the crystallite column-length distribution, calculated by the Warren-Averbach method, can be interpreted as a surface-weighted crystallite-size distribution. This distribution can be considered to be a probability distribution function with frequency equal to the normalized probability of finding a crystallite measuring L (Å) in the [001] direction of diffraction. In this way, the average column length can be interpreted as the mean, surface-weighted crystallite size, equal to the first-order moment (mean value or expected value) of size distribution:

$$\int_0^\infty f(L)dL = \langle L \rangle \qquad (1)$$

The volume-weighted mean crystallite size, obtained by the Voigt-function method, can be calculated from the second-order moment of size distribution, providing complementary characteristics of each investigated sample:

$$\frac{\left(\int_0^\infty L^2 f(L)dL\right)}{\left(\int_0^\infty Lf(L)dL\right)} = \langle D_v \rangle \qquad (2)$$

In Figure 5, an example of measurements performed on an FESEM image of sample K0 is shown. In Table 3 are summarized the main statistics of these measurements for each sample. A clear reduction of average thickness was observed in both series. Dispersion of the

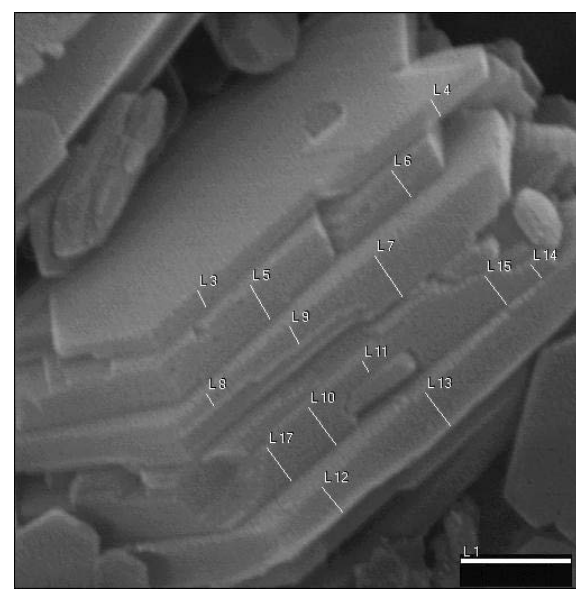

Figure 5. Example of thickness measurements on a photomicrograph of sample K0. Scale bar = 2500 Å.

https://doi.org/10.1346/CCMN.2009.0570102 Published online by Cambridge University Press

Table 3. Results of particle-thickness measurements by FESEM.

Sample	<T> Average thickness value (Å)	σ Standard deviation (Å)	T_{mode} Highest-frequency thickness value (Å)	T_{min} Minimum thickness measured (Å)	T_{max} Maximum thickness measured (Å)	n Number of measurements
K0	662	298	400	170	1623	247
A24	588	304	350	129	2125	363
A60	378	236	150	88	1549	221
S24	346	164	250	106	933	59
S36	152	74	100	66	460	110

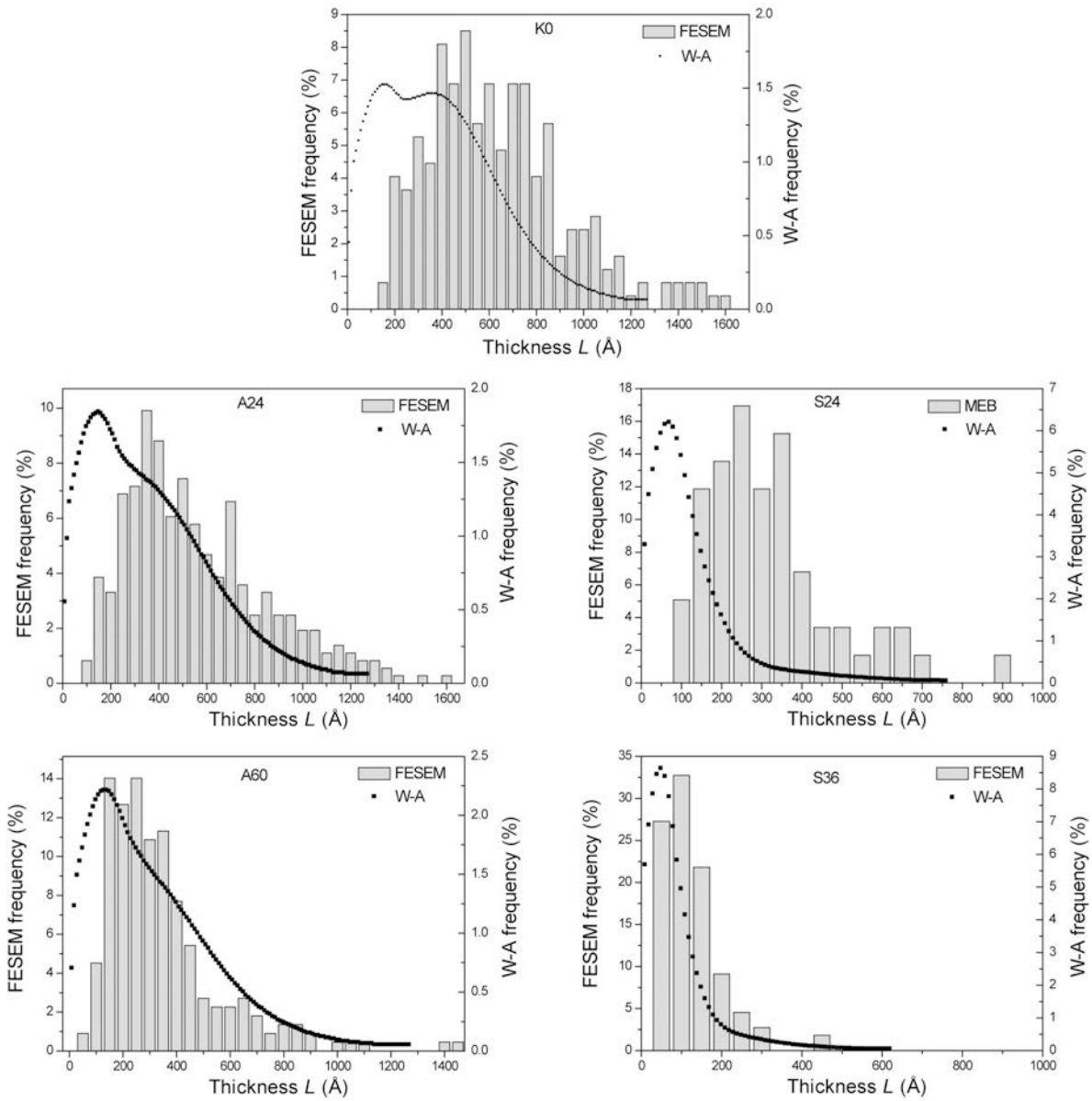

Figure 6. Histograms generated from FESEM particle-thickness measurements superimposed with Warren-Averbach column-length distributions.

https://doi.org/10.1346/CCMN.2009.0570102 Published online by Cambridge University Press

results narrowed, as indicated by the decrease in standard deviation values. In addition, the mode of the thicknesses population shifted to smaller values, and (with one exception) maximum and minimum values also decreased with grinding time.

All these trends were found to be more pronounced in the stainless steel set, as was observed by XRD methods.

The particle thicknesses observed by FESEM were in the range of crystallite sizes perpendicular to (001) observed by Clausell *et al*. (2007). The possibility of having kaolinite particles with a thickness corresponding to the length of a single crystallite in the direction perpendicular to (00l) is supported by this agreement.

The Warren-Averbach column-length distributions were superimposed on histograms generated by FESEM-thickness measurements (Figure 6), with bars 50 Å wide. The histograms are approximately of the same shape (logarithmic-normal) as the crystallite-size distributions, establishing another relationship between [001] crystallite size and particle thickness. Due to the difficulty of observing the smallest and most poorly crystallized particles, FESEM-thickness measurements systematically overestimate the crystallite size, as is clearly visible in samples with a broad particle-size distribution. Remarkably, in wide and clearly bimodal distributions such as K0 and A24, the FESEM frequency

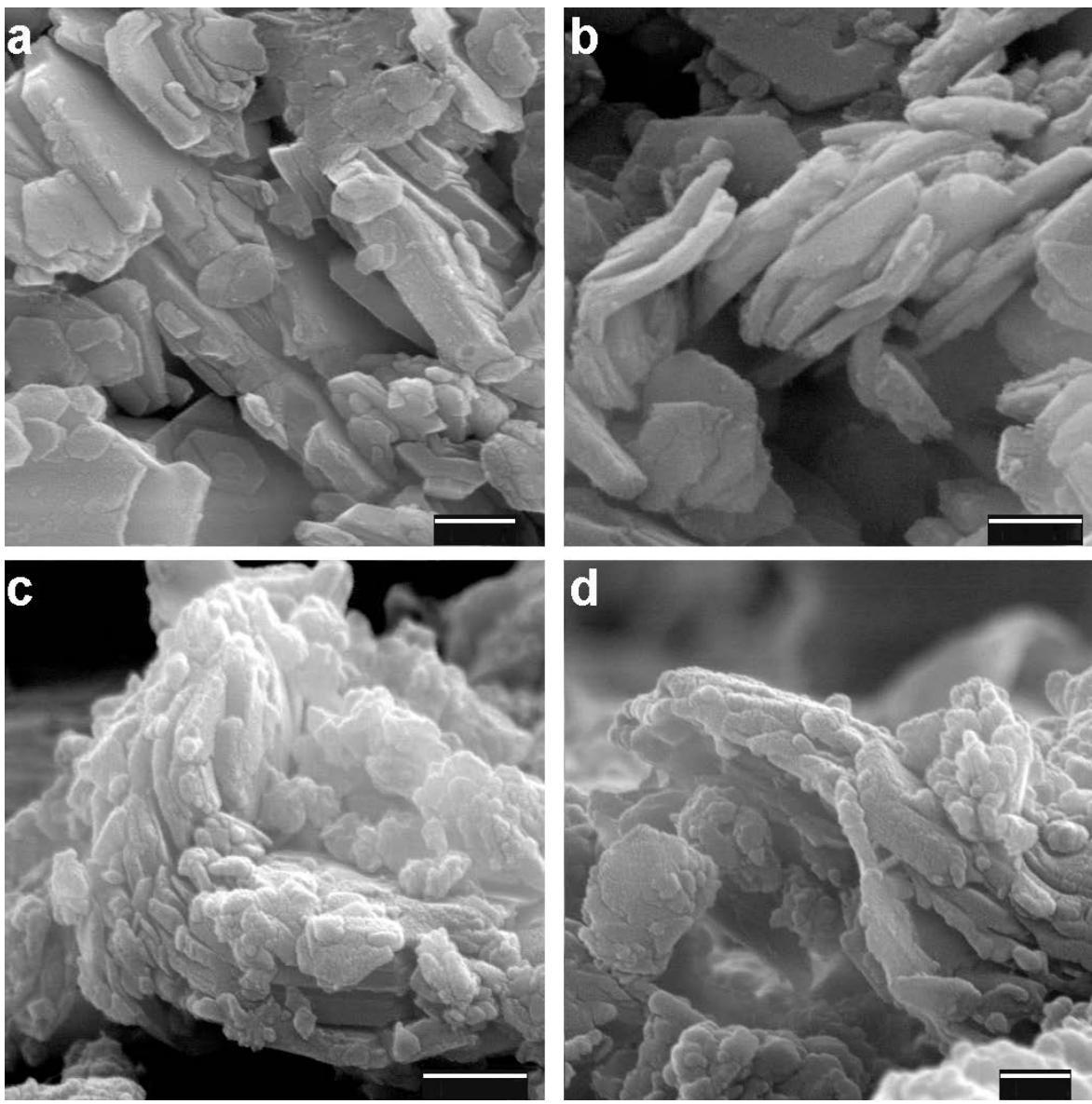

Figure 7. SEM images of samples (a) A24, (b) A60, (c) S24 and (d) S36. Scale bar = 2500 Å (A,B,D) 5000 Å (C).

https://doi.org/10.1346/CCMN.2009.0570102 Published online by Cambridge University Press

main maximum matches the Warren-Averbach secondary maximum. This confirms that greater thicknesses have a greater probability of being observed and measured by FESEM. Nevertheless, in samples with greater milling times and narrower crystallite-size distributions, a good agreement between the FESEM and the Warren-Averbach results can be observed.

Alterations in particle shapes due to the mechanical treatment are clearly visible in micrographs of treated samples (see examples in Figure 7). The sharp edges and angles of well-shaped pseudo-hexagonal particles in the untreated material become irregular and rough after 24 s of milling. For the samples with the longest milling times, for both sets, the edges are smoothed and even bent and broken particles can be found.

CONCLUSIONS

High-energy, vibrating-cup milling using two configurations (agate elements and steel elements) was used for the comminution of a reference kaolinite sample.

Two different methods of XRD microstructural analysis (the Warren-Averbach and the Voigt function methods) were applied successfully to the study of the efficiency of the comminution methods performed in the microstructure of kaolinite.

Although more detailed information (including size and strain distributions) can be obtained using the Warren-Averbach method, the simplified Voigt function method (convenient when only one reflection is available) could also be suitable for crystallite-size determination in kaolinite. A good correlation was observed here between the average apparent crystallite-size values obtained with both methods. The ratios between them also fall within the theoretical range (depending on the Cauchyan contribution to the profile).

The FESEM measurements of kaolinite platelet thickness are reasonably close to [00l] crystallite-size values. Characteristic flakes of kaolinite with basal (001) faces were identified as crystalline grains formed by one layer of crystallites, with approximately the same mean volume-weighted size of both platelets and crystallites in a direction perpendicular to the (001) planes.

A better agreement between FESEM particle-thickness measurements and XRD crystallite-size determination was found for samples with monomodal and narrow crystallite-size distributions.

For strain evaluation, better results were achieved using the Warren-Averbach method, which has been able to distinguish strain values between samples in both treatment series (agate and stainless steel elements), showing an increase in strain with milling time.

For materials processing, vibrating-cup milling has proved to be a more efficient method of comminution of kaolinites than other milling techniques, achieving an extensive degree of microstructural alterations within seconds. Due to its greater mass and volume, the coated stainless steel set has a greater effect on kaolinite microstructure than the agate set, working at the same number of rotations per minute.

ACKNOWLEDGMENTS

The authors are grateful to the reviewers, Peter Uhlik and Éva Makó, and to the Associate Editor, Bruno Lanson, for their helpful comments.

REFERENCES

Balzar, D. and Ledbetter, H. (1993) Voigt-Function modelling in Fourier analysis of size- and strain-broadened X-ray diffraction peaks. *Journal of Applied Crystallography*, **26**, 97–103.

Bastida, J., Kojdecki, M.A., Pardo, P., and Amorós, P. (2006) X-ray diffraction line broadening on vibrating dry-milled two crows sepiolite. *Clays and Clay Minerals*, **54**, 390–401.

Baudet, G., Perrotel, V., Seron, A., and Stellatelli, M. (1999) Two dimensions comminution of kaolinite clay particles. *Powder Technology*, **105**, 125–134.

Bertaut, E.F. (1950) Raies de Debye-Scherrer et Repartition des Dimensions des Domaines de Bragg Dans les Poudres Polycristallines. *Acta Crystallographica*, **3**, 14–18.

Bish, D.L. (1993) Rietveld refinement of the kaolinite structure at 1.5 K. *Clays and Clay Minerals*, **41**, 738–744.

Chipera S.J. and Bish D.L. (2001) Baseline studies of The Clay Minerals Society Source Clays: Powder X-ray diffraction analyses. *Clays and Clay Minerals*, **49**, 398–409.

Clausell, J.V. (2001) Análisis microestructural de caolinita y génesis de caolines en el Macizo Ibérico. *Cadernos Laboratorio Xeoloxico Laxe*, **26**, 11–99.

Clausell, J.V., Bastida, J., Serrano, F.J., Pardo, P., and Huertas, F.J. (2007) A new FESEM procedure for assessment of XRD microstructural data of kaolinites. *Applied Clay Science*, **37**, 127–132.

De Keijser, Th.H., Mittemeijer, E.J., and Rozendaal, H.C.F. (1983) The determination of crystallite-size and lattice-strain parameters in conjunction with the profile-refinement method for the determination of crystal structures. *Journal of Applied Crystallography*, **16**, 309–316.

Eberl, D.D., Drits, V.A., and Środoń, J. (1998) Deducing growth mechanisms for minerals from the shapes of crystal size distributions. *American Journal of Science*, **298**, 499–533.

Frost, R.L., Makó, E., Kristóf, J., Horvath, E., and Kloprogge, J.T. (2001) Modification of kaolinite surfaces by mechanochemical treatment. *Langmuir*, **17**, 4731–4738.

Frost, R.L., Makó, E., Kristóf, J., and Kloprogge, J.T. (2002) Modification of kaolinite surfaces through mechanochemical treatment – A mid-IR and near-IR spectroscopic study. *Spectrochimica Acta – Part A Molecular and Biomolecular Spectroscopy*, **58**, 2849–2859.

Frost, R.L., Horvath, E., Makó, E., and Kristóf, J. (2004) Modification of low- and high-defect kaolinite surfaces: implications for kaolinite mineral processing. *Journal of Colloid and Interface Science*, **270**, 337–346.

González-García, F., Ruiz Abrio, M.T., and González Rodríguez, M. (1991) Effects of dry grinding on two kaolins of different degrees of crystallinity. *Clay Minerals*, **26**, 549–565.

Harben, P.W., and Bates, R.L. (1990) Industrial minerals. Geology and world deposits. *Metal Bulletin PLC*. London, 311 pp.

Klug, H.P. and Alexander, L.E. (1974) *X-ray Diffraction Procedures for Polycrystalline and Amorphous Materials*. John Wiley & Sons, New York, 965 pp.

Konta, J. (1995) Clay and Man – Clay raw-materials in the service of man. *Applied Clay Science* **10**, 275–335.

Kristóf, E., Juhasz, A.Z., and Vassanyi, I. (1993) The effect of mechanical treatment on the crystal-structure and thermal-behavior of kaolinite. *Clays and Clay Minerals* **41**, 608–612.

Langford, J.I. (1978) Rapid method for analyzing breadths of diffraction and spectral-lines using Voigt function. *Journal of Applied Crystallography* **11**, 10–14.

Langford, J.I. (1992) The use of the Voigt function in determining microstructural properties from diffraction data by means of pattern decomposition. Pp. 110–126 in: *Accuracy in Powder Diffraction II* (E. Prince and J.K. Stalick, editors). Special Publication, National Institute of Standards and Technology, Boulder, Colorado, USA, 846 pp.

Makó, E., Frost, R.L., Kristóf, J., and Horvath, E. (2001) The effect of quartz content on the mechanochemical activation of kaolinite. *Journal of Colloid and Interface Science*, **244**, 359–364.

Marchese, J., Almandoz, C., Amaral, M., Palacio, L., Calvo, J.I., Pradanos, P., and Hernandez, A. (2000) Fabrication and characterization of microfiltration tubular ceramic membranes. *Boletin de la Sociedad Española de Ceramica y Vidrio*, **39**, 215–219.

Mermut, A.R. and Cano, A.F. (2001) Baseline studies of The Clay Minerals Society Source Clays: Chemical analyses of major elements. *Clays and Clay Minerals,* **49**, 381–386.

Murray, H.H., Bundy, W.M., and Harvey, C.C. (eds.) (1993) *Kaolin Genesis and Utilization*. Special Publication, **1**, The Clay Minerals Society, Bloomington, Indiana, USA, 341 pp.

Olivier, J.P. and Sennett, P. (1973) Particle size-shape relationships in Georgia sedimentary kaolins II. *Clays and Clay Minerals*, **21**, 403–412.

Pardo, P., Bastida, J., Kojdecki, M.A., Ibáñez, R., and Zbik, M. (2007) X-ray diffraction line broadening in dry grinding of kaolinite. *Zeitschrift für Kristallographie Supplement,* **26**, 549–554.

Pruett, R.J and Webb, H.L., (1993) Sampling and analysis of KGa-1B well-crystallized kaolin source clay. *Clays and Clay Minerals*, **41**, 514–519.

Sanchez-Soto, P.J, de Haro, M.D.J., Perez-Maqueda, L.A., Varona I., and Perez-Rodriguez, J.L. (2000) Effects of dry grinding on the structural changes of kaolinite powders. *Journal of the American Ceramic Society*, **83**, 1649–1657.

Serrano, F.J., Bastida, J., Amigó, J.M., and Sanz, A. (1996) XRD line broadening studies on mullite. *Crystal Research and Technology*, **31**, 1085–1093.

Vogt, C., Lauterjung, J., and Fischer, R.X. (2002) Investigation of the clay fraction (<2 μm) of the Clay Minerals Society reference clays. *Clays and Clay Minerals*, **50**, 388–400.

Warren, B.E. and Averbach, B.L. (1950) The effect of cold-work distortion on X-ray patterns. *Journal of Applied Physics*, **21**, 595–599.

Warren, B.E. (1955) A generalized treatment of cold work in powder patterns. *Acta Crystallographica*, **8**, 483–486.

Zbik, M. and Smart, R.S. (1998) Nanomorphology of kaolinites: Comparative SEM and AFM studies. *Clays and Clay Minerals*, **46**, 153–160.

(*Received 28 August 2007; revised 24 September 2008; Ms. 0061; A.E. B. Lanson*)